



ELSEVIER

Available online at www.sciencedirect.com

SCIENCE @ DIRECT®

Journal of Applied Geophysics 55 (2004) 211–224

JOURNAL OF
APPLIED
GEOPHYSICS

www.elsevier.com/locate/jappgeo

A new method for complete quantitative interpretation of self-potential anomalies

Hesham M. El-Araby

Geology Department, College of Science, King Saud University, P.O. Box 2455, Riyadh 11451, Kingdom of Saudi Arabia

Received 4 March 2003; accepted 17 November 2003

Abstract

A least-squares minimization approach to determine the shape of a buried polarized body from a self-potential (SP) anomaly profile has been developed. By defining the anomaly value at three points on the profile, one at the origin and the others at any two symmetrical points around the origin, the problem of the shape-factor determination is transformed into the problem of finding a solution of a nonlinear equation. Procedures are also formulated to complete the quantitative interpretation by finding the depth, polarization angle, and the electric dipole moment. The validity of the new proposed method has been tested on synthetic data with and without random noise. The obtained parameters are in congruence with the model parameters when using noise free synthetic data. After adding $\pm 5\%$ random error in the synthetic data, the maximum error in model parameters is less than $\pm 5\%$. Moreover, when error in profile origin position determination is studied, the method is approved to be not sensitive to it. Two oft cited field examples from Turkey have also been analyzed and interpreted by the proposed method, where an acceptable agreement has been noticed between the obtained results and other published results. The present method has the capability of avoiding noisy data points and enforcing the incorporation of points free from random errors to enhance the interpretation results.

© 2003 Elsevier B.V. All rights reserved.

Keywords: Self-potential; Interpretation; Least-squares; Model parameters; Shape-factor; Noise

1. Introduction

The self-potential (SP) method has a wide range of applications in Engineering and Geotechnical investigations (Corwin, 1984; Markiewicz et al., 1984), Geothermal exploration (Corwin and Hoover, 1979; Fitterman and Corwin, 1982; Anderson, 1984), cavity detection (Schivavone and Quarto, 1992), and in the exploration for minerals, particularly metallic sulfides (Yüngül, 1950). The self-potential method is based on the measurement of naturally occurring potential dif-

ferences generated mainly by electrochemical, electrokinetic, and thermoelectric sources. Sometimes an individual SP anomaly is found that stands out so clearly that it can be separated from the regional background and the topographic interference, and is so simple in appearance that it can be modeled by a single polarized body. In this case, quantitative methods of interpretation can be used to determine the parameters of the polarized body by assuming a model with simple geometry. The model is considered realistic if the form and magnitude of calculated SP effects are close to the observed anomalies, and the model is geologically reasonable.

E-mail address: hmaraby@hotmail.com (H.M. El-Araby).

Several graphical, and numerical methods have been developed to interpret SP anomalies including curve matching, characteristic points, least-squares, derivative and gradient analysis, nonlinear modeling, and Fourier analysis techniques. Examples of such techniques used for interpreting the self-potential anomalies of horizontal and vertical cylinders, spheres, sheets and geological contacts are classified as follows.

(1) Methods using only a few points on the anomaly curve. These were originally developed by DeWitte (1948), Yüngül (1950), Paul (1965), Paul et al. (1965), Bhattacharya and Roy (1981), Atchuta Rao and Ram Babu (1983). The essential disadvantage of these methods was related to the fact that only a few points are used on the anomaly curve, and hence, the interpreted results are not reliable.

(2) Curve matching techniques. According to Meiser (1962), Satyanarayana Murty and Haricharen (1985), the field curve is compared with sets of theoretical curves either manually or using a computer. This process is cumbersome and the complexity of the method is very high especially when the variables are numerous.

(3) Least-squares methods. Here, the model parameters that give a best fit are derived using an initial presumption, as well as characteristic points and distances from the measured anomaly curve. Examples of these methods are of Abdelrahman and Sharafeldin (1997), Abdelrahman et al. (1997b, 2003).

The above-mentioned three categories have the disadvantage of using characteristic points, distances, curves, and nomograms for interpretation, which is subject to human error in estimating these few points and distances, especially if they are derived by interpolation procedure. This can consequently lead to errors in derived parameters. Moreover, some of these methods demand knowledge of the anomalous body shape, and based on the interpreter's choice, the results could vary a lot.

(4) Methods using derivative analysis and gradients. Namely those of Abdelrahman et al. (1997a, 1998a,b, 2003) belong to this category.

(5) Methods using Fourier analysis and the wave number domain. Particularly those of Atchuta Rao et al. (1982) and Roy and Mohan (1984) belong to this group.

(6) Modeling and Inversion Methods such as those given by Guptasarma (1983), Furness (1992), and Shi and Morgan (1996).

The last three categories are greatly influenced by noise in measured data and can lead to serious errors.

In this paper, a new method is developed to overcome almost all of the above-mentioned drawbacks, especially the handling of random errors and noisy data. So, a least-squares minimization approach is formulated to determine the shape factor using all data points on a self-potential anomaly profile, without the need for any characteristic distances. The only requirement of this method like the previous ones is the placement of the data profile origin over the center of the body. Practically, this is just to place $x_i = 0$ of the profile above the origin of the body to start data digitization. This new method resembles the least-squares methods but it does not need any measure of characteristic distances to operate like them (e.g. no need for x_0 distance which is measured from the origin of the profile to the point of the zero anomaly). The problem of shape factor estimation is transformed into the question of finding a solution of a nonlinear equation of the form $f(q) = 0$. A procedure is derived to parameterize the depth, polarization angle, and the electric dipole moment in order to determine their values. The method has been applied to synthetic data with and without random errors, and has been tested on two field examples from Turkey.

2. Formulation of the problem

The general self-potential (SP) anomaly expression produced by most polarized structures along a principal profile over the body is given by the following equation at a point $P(x_i, z)$ (Fig. 1) (Yüngül, 1950; Bhattacharya and Roy, 1981; Satyanarayana Murty and Haricharen, 1985; Abdelrahman et al., 1998a).

$$V(x_i, z, \theta, q) = k \frac{x_i \cos \theta + z \sin \theta}{(x_i^2 + z^2)^q},$$

$$i = -N, \dots, -1, 0, 1, \dots, N \quad (1)$$

where z is the depth, θ is the polarization angle between the axis of polarization ξ and the horizontal, x_i is a discrete point along x -axis where the observed anomaly is located, q is the shape-factor which

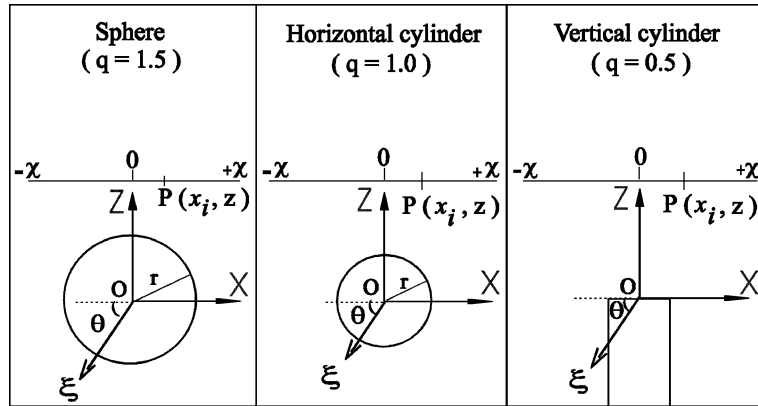


Fig. 1. Cross-sectional view of the sphere, horizontal and vertical cylinder models.

defines the geometry of the source body, and k is the electric current dipole moment or the magnitude of polarization which depends on the shape of the body (e.g. for a sphere $k = Er^2$, where E is the electromotive force and r is the radius of the sphere). The units of k change with the model shape to maintain the Volt units of the potential in Eq. (1). The shape-factors for a sphere (3-D), a horizontal cylinder (2-D) and a semi-infinite vertical cylinder (3-D) are 1.5, 1.0 and 0.5, respectively.

For all shapes (a function of q), Eq. (1) gives the following relationship at the origin ($x_i = 0$):

$$V(0) = k \frac{\sin\theta}{z^{2q-1}} \quad (2)$$

where $V(0)$ is the anomaly value at the origin. Consequently,

$$k = V(0) \frac{z^{2q-1}}{\sin\theta}, \quad \sin\theta \neq 0 \quad (3)$$

Replacing k in Eq. (1) with the above formula will eliminate the unknown k by introducing the known value of $V(0)$ along the measured profile at the origin and would give the following equation:

$$V(x_i, z, \theta, q) = V(0) z^{2q-1} \frac{x_i \cot\theta + z}{(x_i^2 + z^2)^q} \quad (4)$$

Let us consider two observation points ($x_i = -s$ and $x_i = s$) along the anomaly profile, where $s = 1,$

$2, \dots, M$ spacing units. These two known measured values $V(s)$ and $V(-s)$ will be used to reduce the number of the three unknowns in Eq. (4) (z, θ, q) to one unknown which is q . Using Eq. (4), the self-potential anomaly at these two points is given by:

$$V(s) = V(0) z^{2q-1} \frac{s \cot\theta + z}{(s^2 + z^2)^q} \quad (5)$$

$$V(-s) = V(0) z^{2q-1} \frac{z - s \cot\theta}{(s^2 + z^2)^q} \quad (6)$$

From Eqs. (2), (5) and (6), we obtain the following two relations:

$$F = \frac{z^{2q}}{(s^2 + z^2)^q} \quad (7)$$

where: $F = [V(s) + V(-s)]/[2V(0)]$

$$P = \frac{s z^{2q-1}}{(s^2 + z^2)^q} \cot\theta \quad (8)$$

where: $P = [V(s) - V(-s)]/[2V(0)]$

F and P are two known numerical quantities that should be calculated using the measured self-potential anomaly at three points on the profile where $x = 0$ and $x = \pm s$ in order to be incorporated in the solution for q instead of the unknowns z and θ .

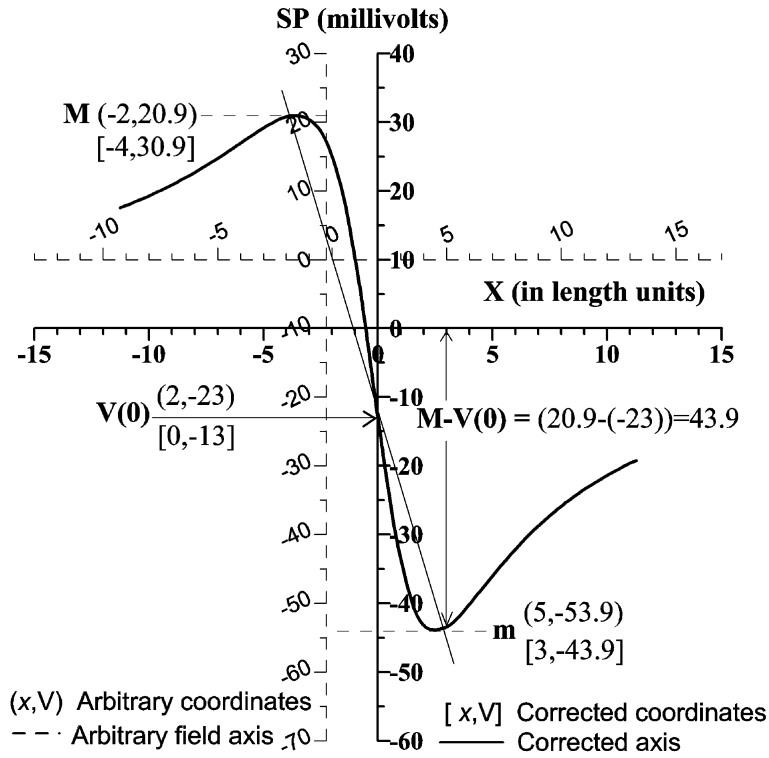


Fig. 2. A typical self-potential anomaly profile over a horizontal cylinder. Identified on this profile are the maximum value (M) and the minimum value (m) from which the origin of the profile and the anomaly value at the origin $V(0)$ can be determined using Stanley's (1977) method.

From Eqs. (7) and (8), we obtain separate formula for z and θ , respectively, as follows:

$$z = \sqrt{\frac{s^2 F^{1/q}}{1 - F^{1/q}}} \quad (9)$$

$$\cot\theta = \frac{P}{sF} \sqrt{\frac{s^2 F^{1/q}}{1 - F^{1/q}}} \quad (10)$$

Substituting Eqs. (9) and (10) into Eq. (4), we obtain the following nonlinear equation in q as shown in Appendix A.

$$V(x_i, q) = V(0)W(x_i, q) \quad (11)$$

where

$$W(x_i, q) = s^{2q-1} \frac{x_i P + sF}{[x_i^2 + F^{1/q}(s^2 - x_i^2)]^q}$$

The unknown shape-factor q in Eq. (11) can be obtained by minimizing

$$\phi(q) = \sum_{i=-N}^N [Y(x_i) - V(0)W(x_i, q)]^2 \quad (12)$$

with respect to q in a least-squares sense. $Y(x_i)$ denotes the measured observed SP anomaly at x_i .

Minimization of $\Phi(q)$ in the least-squares sense involves setting the derivative of $\Phi(q)$ with respect to q equal to zero and leads to the following equation

$$f(q) = \sum_{i=-N}^N [Y(x_i) - V(0)W(x_i, q)]W'(x_i, q) = 0 \quad (13)$$

where

$$W'(x_i, q) = \frac{d}{dq} W(x_i, q)$$

Eq. (13) can be solved for q using standard methods for solving systems of nonlinear equations. Here, the simple iteration method described by [Demidovich and Maron \(1973\)](#) is used. First, Eq. (13) will be transformed into the form of $q=f(q)$ as shown in Appendix B to give the following equation:

$$q = \frac{\sum_{i=-N}^N V(0)W^2(x_i, q) \left\{ \frac{(s^2 - x_i^2)F^{1/q} \ln F}{x_i^2 + F^{1/q}(s^2 - x_i^2)} \right\}}{\sum_{i=-N}^N Y(x_i)W'(x_i, q) - \sum_{i=-N}^N V(0)W^2(x_i, q) \ln \left\{ \frac{s^2}{x_i^2 + F^{1/q}(s^2 - x_i^2)} \right\}} \quad (14)$$

then, it is transformed into the following iterative form

$$q_c = f(q_i) \quad (15)$$

where q_i is the initial shape-factor and q_c is the calculated revised shape-factor. q_c is used as q_i for the next iteration. The iteration stops when $|q_c - q_i| \leq e$, where e is a small predetermined real number close to zero. So the source shape-factor is determined by solving one nonlinear equation in q . Any initial guess for q works well because there is only one global minimum.

Once q is known, the depth z can be determined from Eq. (9), and the polarization angle θ from Eq. (10). Knowing z , θ , and q , the electric dipole moment k can be determined from Eq. (3).

3. Locating the origin of the profile

To this stage, we have assumed knowledge of the axes of the SP profile so that $V(0)$ can be determined. In practice, the selected anomaly profile should always be the straight line between the negative and positive centers of the anomaly. This is acceptable to be in the direction of the polarization plane, which is the vertical plane passing through the axis of polarization. A field traverse along this line will have an arbitrary origin, in which case the position of the structure ($x_i = 0$) must first be determined. The origin of the profile may readily be located from positions of turning points ([Stanley, 1977](#); [Satyanarayana Murty and Haricharen, 1985](#); [Abdelrahman et al., 1997b, 1999](#)). It is notable that Eq. (1) is the same as the vertical component magnetic anomaly expression due to infinite inclined sheet model. Therefore, the available methods of magnetic interpretation can be adopted here to solve certain SP parameters. For example, $M + m = V(0)$, thus, the origin can be located. Or draw a straight line joining the maximum value (M) to the minimum value (m) of the SP anomaly profile and locate the vertical axis [$x_i = 0$ and $V(0)$] by its intersection with the anomaly curve, irrespective of the profile scale ([Fig. 2](#)). This determines the origin accurately in case of a horizontal cylinder. However, in other cases, [Stanley's method \(1977\)](#) would give

Table 1
Synthetic examples

| Using noise free data | | Using data with $\pm 5\%$ random error | | | | | | | |
|---|------------------|--|-------------------|-------|-------------------|----------|------------------------|---------|-------------------|
| Model shape factor (q) | Computed (q) | q | % of error in q | z | % of error in z | θ | % of error in θ | k | % of error in k |
| <i>Case I: $z = 2$ units, $\theta = 30^\circ$</i> | | | | | | | | | |
| 0.5 | 0.50 | 0.490 | -2.00 | 1.951 | -2.45 | 30.6° | 2.00 | -306.40 | 2.13 |
| 1.0 | 1.00 | 1.006 | 0.60 | 2.048 | 2.41 | 29.8° | -0.66 | -308.13 | 2.71 |
| 1.5 | 1.50 | 1.487 | -0.87 | 2.004 | 0.21 | 30.5° | 1.66 | -293.07 | -2.31 |
| <i>Case II: $z = 2$ units, $\theta = 60^\circ$</i> | | | | | | | | | |
| 0.5 | 0.50 | 0.482 | -3.60 | 2.033 | 1.65 | 61.8° | 3.00 | -305.70 | 1.90 |
| 1.0 | 1.00 | 0.989 | -1.10 | 1.994 | -0.30 | 60.2° | 0.33 | -295.43 | -1.52 |
| 1.5 | 1.50 | 1.510 | 0.66 | 2.027 | 1.35 | 59.7° | -0.50 | -309.00 | 3.00 |
| <i>Case III: $z = 4$ units, $\theta = 30^\circ$</i> | | | | | | | | | |
| 0.5 | 0.50 | 0.485 | -3.00 | 3.896 | -2.60 | 30.7° | 2.33 | -293.2 | -2.26 |
| 1.0 | 1.00 | 1.013 | 1.30 | 4.106 | 2.65 | 29.5° | -1.66 | -308.9 | 2.97 |
| 1.5 | 1.50 | 1.510 | 0.66 | 4.005 | 0.13 | 29.7° | -1.00 | -307.6 | 2.53 |

$K = -300$, profile length = 30 units, sampling interval = 1 unit, and $s = 5$ units.

the approximate location of the origin. The effect of the error in origin location on the proposed method will be discussed in detail later in the theoretical examples section. If there is no maximum defined, then θ reaches 90° and $x = 0$ at the minimum of the

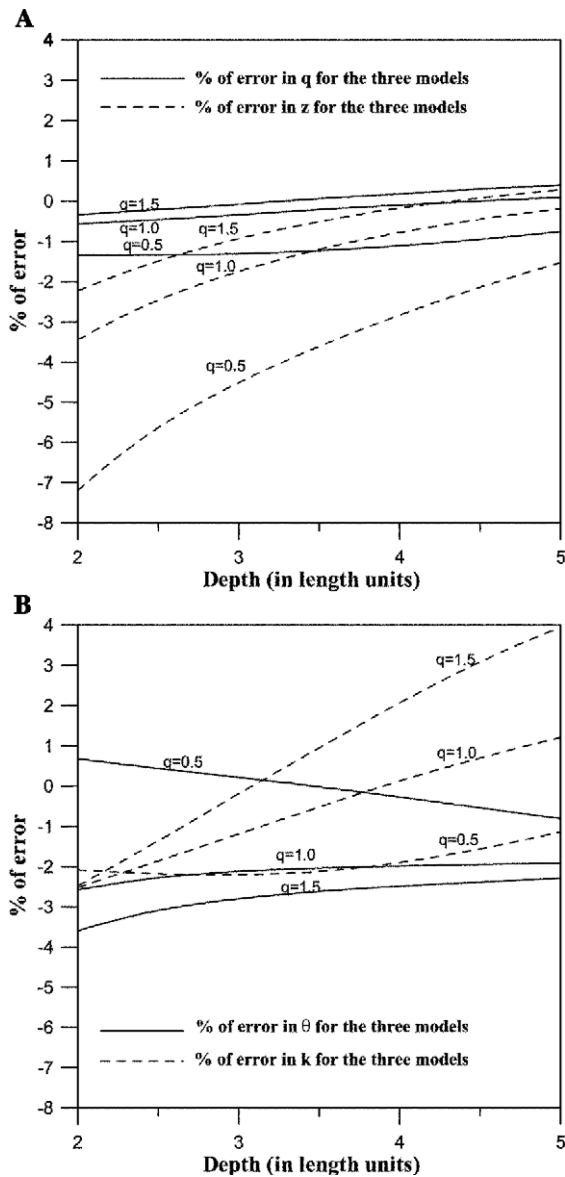


Fig. 3. Error response in model parameters estimates as a function of depth for the noisy data of the three bodies. The other parameters are kept constant (No. of data points = 31, $k = -300$, $\theta = 30^\circ$, and $s = 14$). (A) Error in calculated q and z , (B) error in calculated θ and k .

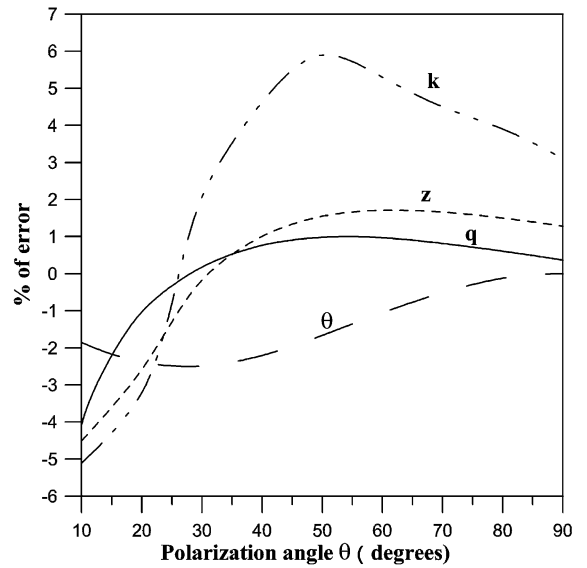


Fig. 4. Error response in model parameters estimates as a function of polarization angle for the noisy data of a sphere model. The other parameters are kept constant (No. of data points = 31, $k = -300$, $z = 4$, and $s = 14$).

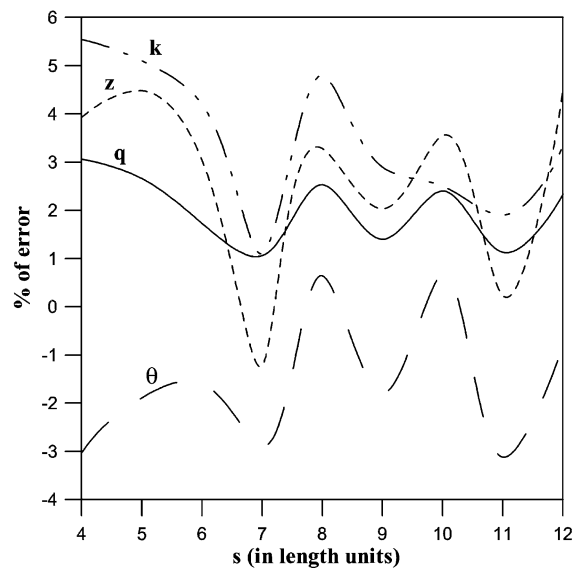


Fig. 5. Error response in model parameters estimates versus (s) values for the noisy data of a horizontal cylinder model. The other parameters are kept constant (No. of data points = 31, $k = -300$, $z = 4$, and $\theta = 30^\circ$).

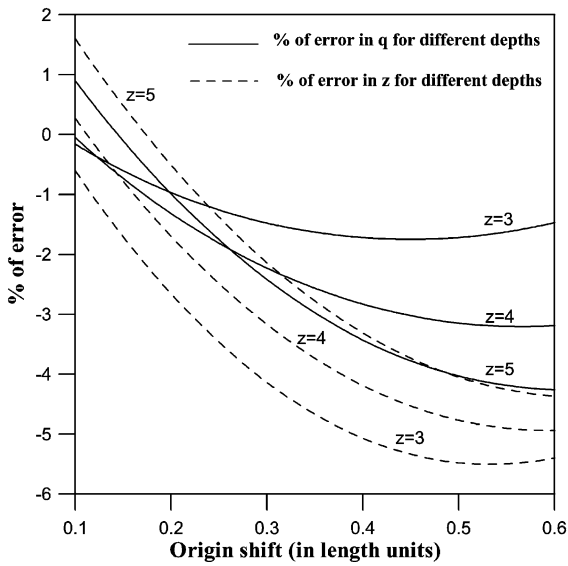


Fig. 6. Error response in calculated q and z parameters as a function of adding different shift amounts in origin position determination for the noisy data of a horizontal cylinder model. For three different depths $z=3, 4,$ and 5 , the other parameters are kept constant (No. of data points = 31, $k=-300$, $\theta=60^\circ$, and $s=4$).

profile. If there is no minimum defined, then θ reaches 270° and $x=0$ at the maximum. The base line, which represents the abscissa of the profile with origin defined relative to the structure, is then constructed a distance $[M - V(0)]$ above the minimum of the profile (Fig. 2).

4. Theoretical examples

Numerical results for various test cases including a vertical cylinder ($q=0.5$), horizontal cylinder ($q=1.0$) and sphere ($q=1.5$) models are shown in Table 1. These verify that the proposed method gives exact values for q, z, θ and k when using noise free data. After adding different sets of random noise within $\pm 5\%$, the maximum error in all derived parameters for small and moderate depths is within $\pm 3\%$, while for large depths, it may reach $\pm 5\%$. However, in studying the error response of the proposed method for different depths and polarization angles, synthetic examples contaminated with the same set of $\pm 5\%$ random errors were consid-

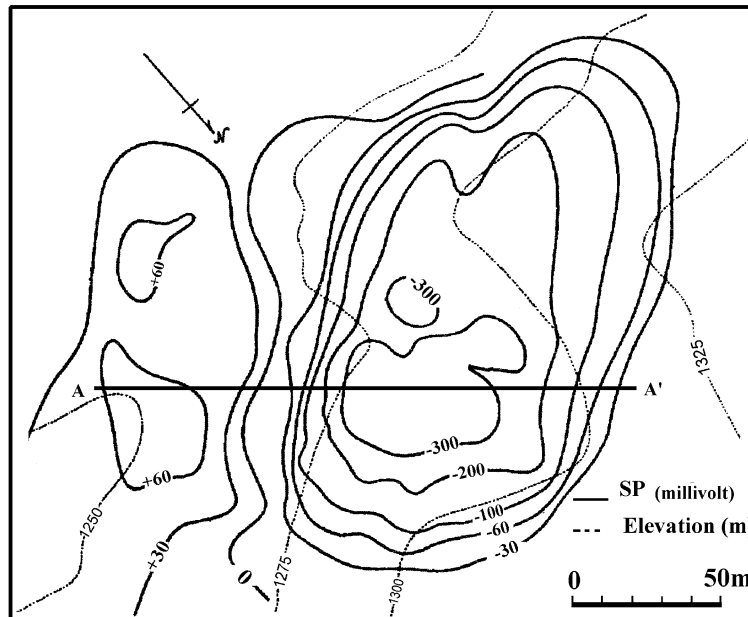


Fig. 7. Weiss SP anomaly, Ergani, Turkey (Yüngül, 1950).

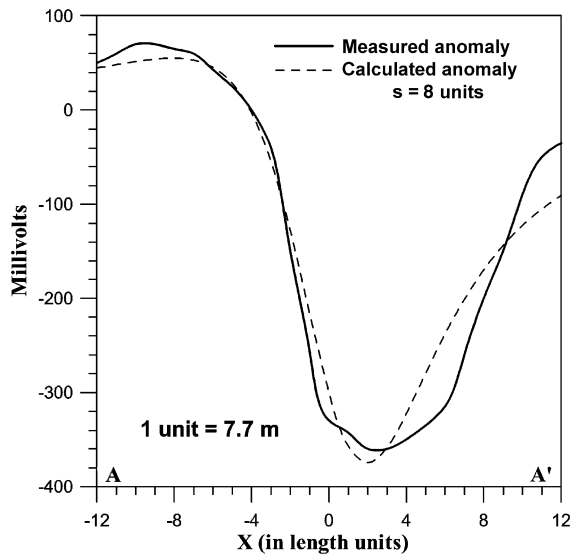


Fig. 8. Measured and calculated SP anomaly along AA' over the Weiss anomaly, Ergani, Turkey.

ered. Following the interpretation procedure, values of the model parameters (q , θ , z , k) for the three model shapes were computed and the percentages of error in them were plotted against the model depth in Fig. 3a and b. While in Fig. 4, the percentage of error in model parameter determination is plotted against the polarization angle for the sphere model. All curves show good results indicated by the acceptable percentage of error range in the calculated model parameters.

Let us consider the possibility of using different pairs of points ($x = \pm s$) in the interpretation procedure, and carry out a similar investigation for the percentage of error in model parameters determination for the sphere model as an example using the same set of $\pm 5\%$ random errors versus different s values. Fig. 5 shows that the method gives good results for a wide

range of s values. It is recognizable that the percentage of error for the four parameters (q , z , θ , k) are related to each other; depending on the random error value hidden in the used pair of points at $x = \pm s$, and varying from one pair to another in the same manner. This gives us the capability of reaching a good solution for the four parameters together once we use the pair of points that has the lowest value of random error.

The proposed method begins with selecting the origin using Stanley's method (1977) and may lead to errors in the solution for q , z and other parameters when real data is being interpreted. To explore the error behavior of such inaccurate origin position determination, errors of 0.1, 0.2, ... 0.6 units are introduced to a sphere model coordinate (x_i) in Eq. (1) for $z = 3, 4$, and 5 and keeping other parameters constant. Then the same interpretation procedure to evaluate the percentage of error in the calculated q and z was followed. The results in Fig. 6 are generally in good agreement with the model parameters and the percentage of error in the calculated q and z are within the minimum range of acceptable percentage of error ($\approx \pm 5\%$).

This illustrates that this new method is not very sensitive to errors in the SP anomaly, and hence, it should provide reliable model parameter estimates when dealing with field data even when the origin is determined approximately using Stanley's (1977) method.

5. Field examples

To examine the applicability of the present method, the following two field examples from the Ergani Copper District, 65 km Southeast of Elazing in Eastern Turkey are presented. The SP measurements were performed and described by Yüngül (1950) and

Table 2
Interpretation of Weiss self-potential anomaly, Ergani copper district, Turkey

| s (units) | Computed shape factor (q) | % of error in computed (q) | Computed depth (z) (m) | Computed polarization angle (θ) (deg) | Computed electrical dipole moment (k) | Root mean square error (RMS) (mV) |
|----------------|-------------------------------------|--------------------------------------|----------------------------------|--|---|---|
| 4 | 1.560 | 4.00 | 42.271 | 36.08° | -21314.9 | 65.99 |
| 6 | 1.691 | 12.73 | 54.469 | 32.80° | -66206.0 | 327.93 |
| 8 | 1.464 | -2.40 | 43.373 | 35.89° | -16256.8 | 32.64 |

Table 3
Comparison of Weiss self-potential anomaly interpretation results derived by different methods

| Parameter | Method of Yüngül (1950) | Method of Bhattachary and Roy (1981) | Method of Abdelrahman and El-Araby (1996–1997) | Method of Abdelrahman et al. (1997a) | Method of Abdelrahman et al. (1998a) | The present method |
|-------------------|--|--------------------------------------|--|---|--------------------------------------|--------------------------------------|
| z | 53.8 m Depth calculated to the center of a sphere | 54 m | 52.9 m | 26 m to the top of a vertical cylinder | 12.7 m | 43.37 m to the center of a sphere |
| θ | 40° | 30° | 35.3° | – | – | 35.89° |
| k | – | – | – | – | – | –16256.8 |
| q | – | – | – | 0.75 estimated as a vertical cylinder | 0.37 | 1.464 estimated as a sphere |
| % of error in q | – | – | – | 50.0 | –26.0 | –2.4 |

then used by many authors to test their proposed methods in many journals.

5.1. Weiss anomaly

The Weiss anomaly is 1 km northwest of the Maden copper mine, where open-cut mining was being conducted. The field example was interpreted by Yüngül (1950), Bhattacharya and Roy (1981), Abdelrahman and El-Araby (1996–1997), Abdelrahman et al. (1997a, 1998a). Fig. 7 shows the Weiss self-potential anomaly map, where the anomaly contour lines are nearly circular in shape indicating a spherical source. A self-potential profile of 192.5-m length along line AA' of this map shown in Fig. 8 was digitized at 25 points at an interval of 7.7 m. The model parameters (q , z and k) obtained by the

proposed method, using three different values of s , are given in Table 2. The comparison between the three computed anomalies based on these derived parameters is carried out through the study of the root mean square error (RMS). This is a measure of how close the calculated model response is to the measured data. It has the same units as the SP anomaly. The lowest relative value is chosen to indicate the most reliable calculated parameters.

$$RMS = \sqrt{\frac{\sum_{i=-N}^N [Y(x_i) - V(x_i, z, \theta, q)]^2}{2N + 1}} \tag{16}$$

Here, $2N + 1$ is the number of observation points. $Y(x_i)$ and $V(x_i, z, \theta, q)$ are the observed and computed SP

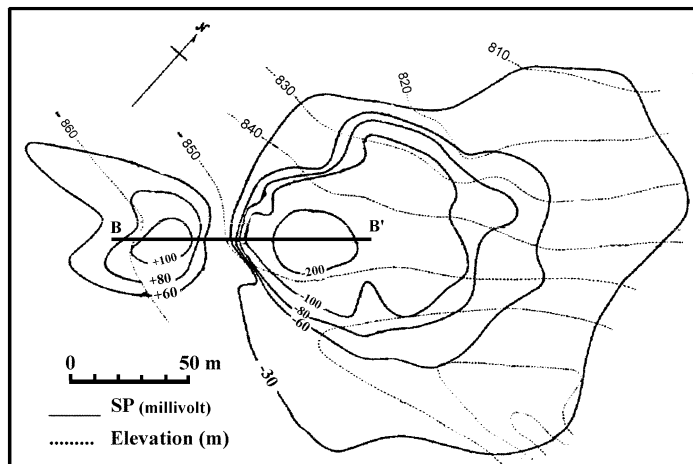


Fig. 9. Süleymanköy SP anomaly, Ergani, Turkey (Yüngül, 1950).

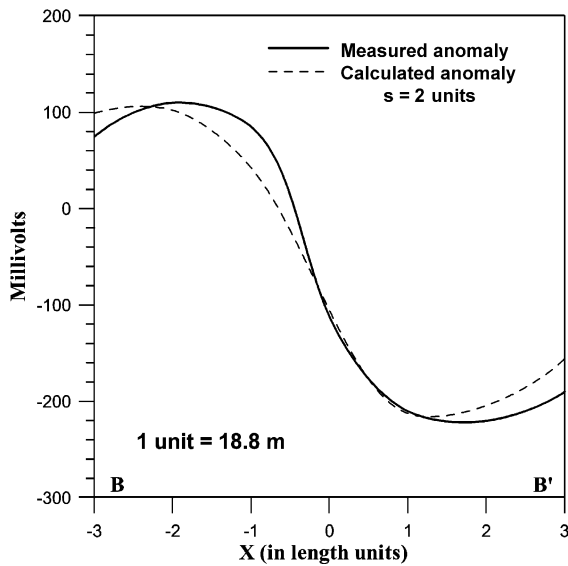


Fig. 10. Measured and calculated SP anomaly along BB' over the Süleymanköy anomaly, Ergani, Turkey.

respectively. This computed error function is equal to 65.99, 327.93 and 32.64 for $s=4$, $s=6$ and $s=8$, respectively. This indicates that the model parameters estimated using $s=8$ produce an SP anomaly closest to the observed one (Fig. 8). This finding also goes well with the obtained results for the percentage of error in estimated q (Table 2). Here the case of $s=8$ has also the smallest percentage of error in calculated q , assuming the true value of q is the nearest exact value of q to the calculated one (in this case, exact $q=1.5$).

It is worth mentioning here that real bodies can adopt any number in between the multiples of 0.5 for

the exact q (shape factor). However, the closest exact value of q to the calculated one gives us the indication to the shape of the model that should be used in further calculations of the rest of the unknown parameters. This helps a lot to reach a good model estimate concentrating on one shape only and leading easily to the smallest root mean square error between the measured and calculated data. This does not mean that the Weiss anomaly is due to a perfect sphere model, but the choice of the sphere model is just an approximation that gives the best fitting model with the most reliable model parameters.

Some misfit between computed and field data is expected due to geologic and measurement noise. The great advantage of the proposed method, is the use of all data points on the measured profile to estimate q and at the same time it gives much weight for two points ($x=\pm s$) to be incorporated into the calculation of the derived parameters. By using the root mean square error function as described above, we can exclude those pairs of points for which the calculated and measured anomalies disagree due to noise, and select the pairs that give a close fit indicating that they are almost free from noise.

The model parameters determined are: $q=1.464$, $z=43.373$ m, $\theta=35.89^\circ$ and $k=-16256.8$. The results agree well with those obtained by different authors (see Table 3).

5.2. Süleymanköy anomaly

Fig. 9 shows the Süleymanköy SP anomaly map which represent the anomaly due to a nearly spherical polarized copper ore body. A self-potential profile of

Table 4

Comparison of Süleymanköy self-potential anomaly interpretation results derived by different methods

| Parameter | Method of Yüngül (1950) | Method of Bhattachary and Roy (1981) | Method of Abdelrahman and Sharafeldin (1997) | Method of Abdelrahman et al. (1997a) | Method of Abdelrahman et al. (1997b) | The present method |
|------------------------------|-------------------------|--------------------------------------|--|--------------------------------------|--------------------------------------|--------------------|
| z | 38.80 m | 40.00 m | 42.00 m | 49.00 m | 38.78 m | 47.63 m |
| θ | 11.00° | 15.00° | 13.00° | – | 14.67° | 14.74° |
| k | – | – | –2458.0 mV | – | –1549.3 mV | –2661.2 mV |
| q | – | – | – | 1.5 | 1.356 | 1.468 |
| Root mean square error (RMS) | – | – | 24.735 | – | 40.998 | 23.672 |

112.8-m length along the line BB' of this map, shown in Fig. 10, was digitized at an interval of 18.8 m. The best obtained root mean square error value is 23.672 for $s=2$. The determined model parameters are $q=1.468$, $z=47.63$ m, $\theta=14.74^\circ$ and $k=-2661$. Table 4 shows the agreement of these model parameters with those obtained by other methods along with an indication of the root mean square error function (RMS) for those methods that were able to determine all model parameters. It is clear that the proposed method gives the best fit solution.

It is evident from the field examples that the present method yields good insight from SP data concerning the nature of the source body. Finally, these field examples emphasize one of the principal advantages of the least-squares methods. A reliable shape-factor can be obtained in spite of irregularities in the anomaly curve that would more seriously affect methods of shape-factor estimation, based on only a few isolated points and distances taken from the anomaly profile.

6. Discussion of the results

It was verified numerically that the proposed method gives exact values for model parameters when using synthetic noise free data. After adding $\pm 5\%$ random error in the synthetic data, the percentage of error in the derived model parameters is within $\pm 3\%$ for small and moderate depths, and it may reach $\pm 5\%$ for large depths.

This new method uses all available data points on the measured SP profile which is an advantage of the present approach compared to the conventional methods that used only some points and distances from the supplied data. However, the power of this method is also apparent for short profile lengths as in the case of Süleymanköy anomaly. The advantage of using all data points is to provide the best fitting solution for all measurement points. However, the use of a chosen pair of points at $x=\pm s$ in estimating the model parameters, gives more weight to these two specific points. The choice of these two points could be changed until the solution reaches the best fit indicated by the root mean square error function. It is also indicated by how close the calculated q value is to the nearest exact value of q . This gives flexibility to judge

and exclude solutions produced from noisy data points and approve others that are derived from points free of noise. This is illustrated very clearly by close examination of the Weiss anomaly case, where for $s=6$, the measured data points at $x=\pm 6$ is poorly fitted by the best fitting model results, indicating that it was not a good choice for model parameter calculation as indicated by the largest root mean square error value. This means that the measured data points at $x=\pm 6$ are contaminated with noise.

A comparison of the derived results by this method with the previous works in the case of the field examples shows that the results are in good agreement. Moreover, the derived results are more acceptable than those obtained by other methods in terms of the behavior of the root mean squares error function (Table 4).

Those methods which are able to obtain all model parameters such as described by Abdelrahman and Sharafeldin (1997), Abdelrahman et al. (1997b, 2003) are influenced by the estimation of the zero anomaly distance x_0 from the origin. This is dependent on the interpreter's choice of the interpolation method to locate this distance between the measured data points. Even if it gives a good result as in the case of Abdelrahman and Sharafeldin (1997) for the Süleymanköy anomaly, this will not mean that it will be as successful for other cases due to the expected error in x_0 . The proposed method has no such drawback because it does not need any distance measurements along the SP profile. On the contrary, the interpreter is able to orient the calculations by excluding bad noisy data through the use of the root mean square error function.

A clear example of the noise effect is recognizable in the interpretation of the Weiss anomaly by Abdelrahman et al. (1997a, 1998a) in terms of a vertical cylinder instead of a sphere. In the latter method, the estimated shape-factor was in the range of $0.52 > q > 0.32$ and the estimated depth range was $17.2 > z > 8.2$ m. The solution was just a graphical central point for these ranges without any measures for the misfits between the observed and calculated anomaly. In the former method, the range was also wide and the choice of the solution was also arbitrary and graphically driven. The interpretation results of these two methods were in contrast with and against the derived results of all other works. This is due to the magnification of the noise

through their methods of gradient and derivative analysis. This also applies to the higher derivatives method of Abdelrahman et al. (2003).

The presented new method is designed specially to handle such problems concerning random errors and noise in acquired self-potential data during the interpretation process.

7. Conclusions

The present new method has succeeded in solving the problem of determining the shape of a buried structure (shape-factor) from self-potential data along a short profile running between the maximum and minimum of the anomaly. The formulation of the problem was capable of transforming this issue into the problem of finding a solution of a nonlinear equation. A least-squares minimization approach is formulated to use all data points, in addition to a pair of measured data points (at $x = \pm s$) which grant weight to these selected points that could be free of noise. Repetition of the method for different such pairs of measured points will lead to the best fitting model. This happens when this pair of points contain the least amount of noise in the whole set of measured data. Procedures are also given to calculate the rest of the model parameters including the depth, polarization angle and electric dipole moment. The method presented here is very simple to execute. It does not depend on the shape of the model and approved to be stable for a wide range of depths and polarization angles. The advantages of the proposed method over previous techniques which use a few points, distances, derivatives and gradient analysis, are (1) all observed values can be used, (2) the method is automatic, (3) the method is less sensitive to errors in the SP anomaly and (4) it does not need any distance measurements on the anomaly profile. It is also emphasized that the present method can be used to gain geologic insight into the subsurface, as illustrated by the field examples.

Acknowledgements

The author thanks the reviewers and editors especially Prof. Andreas Hördt for his excellent

suggestions that improved the original manuscript. I would like to acknowledge the constructive comments of Prof. El-Sayed Abdelrahman, Chairman, Geophysics Department, Cairo University. The author also thanks Dr. Abdulaziz Al-Bassam (Vice Dean, College of Science, King Saud University) and Dr. Nassir Al-Arifi (Chairman, Geology Department, King Saud University) for their continuous support.

Appendix A. Derivation of Eq. (11)

Upon substituting $\cot \theta$ in Eq. (4) by its equivalent in Eq. (10), we get:

$$V(x_i, z, q) = V(0)z^{2q-1} \frac{x_i \frac{Pz}{sF} + z}{(x_i^2 + z^2)^q} \quad (17)$$

$$V(x_i, z, q) = V(0) \frac{z^{2q}}{sF} \frac{x_i P + sF}{(x_i^2 + z^2)^q} \quad (18)$$

Using the equivalent form of F given in Eq. (7), we get:

$$V(x_i, z, q) = V(0) \frac{(s^2 + z^2)^q}{s} \left[\frac{x_i P + sF}{(x_i^2 + z^2)^q} \right] \quad (19)$$

On replacing z by Eq. (10), the following equation is obtained:

$$V(x_i, q) = V(0) \frac{\left(s^2 + \frac{s^2 F^{1/q}}{1 - F^{1/q}} \right)^q}{s} \left[\frac{x_i P + sF}{\left(x_i^2 + \frac{s^2 F^{1/q}}{1 - F^{1/q}} \right)^q} \right] \quad (20)$$

$$V(x_i, q) = V(0) \frac{[s^2(1 - F^{1/q}) + s^2 F^{1/q}]^q}{s} \times \left\{ \frac{x_i P + sF}{[x_i^2(1 - F^{1/q}) + s^2 F^{1/q}]^q} \right\} \quad (21)$$

This leads directly to Eq. (11).

Appendix B. Derivation of Eq. (14)

First the derivative of Eq. (11) $W(x_i, q)$ should be derived. Let us assume that:

$$\left. \begin{aligned} \alpha &= (x_i P + sF), \\ \beta &= (s^2 - x_i^2), \\ \gamma &= x_i^2, \\ a &= s, \\ b &= F \\ x &= q \end{aligned} \right\} \quad (22)$$

Now we reach the equivalent equation for W in terms of a variable x instead of q :

$$W(x) = \frac{\alpha - a^{2x-1}}{[\gamma + \beta - b^{1/x}]^x} \quad (23)$$

To get $W' = dW/dx$, let's first modify the above equation as follows:

$$W[\gamma + \beta - b^{1/x}]^x = \alpha - a^{2x-1} \quad (24)$$

Applying the logarithm on both sides, we obtain the following:

$$\begin{aligned} \ln(W) + x - \ln(\gamma + \beta - b^{1/x}) \\ = \ln(\alpha) + (2x - 1)\ln(a) \end{aligned} \quad (25)$$

By differentiating both sides, we get:

$$\begin{aligned} \frac{1}{W} W' + x \left[\frac{1}{(\gamma + \beta b^{1/x})} \left(\frac{-\beta b^{1/x} \ln(b)}{x^2} \right) \right] \\ + \ln(\gamma + \beta b^{1/x}) = 2\ln(a) \end{aligned} \quad (26)$$

$$\begin{aligned} W' = W \left\{ 2\ln(a) - \ln(\gamma + \beta b^{1/x}) \right. \\ \left. - x \left[\frac{1}{(\gamma + \beta b^{1/x})} \left(\frac{-\beta b^{1/x} \ln(b)}{x^2} \right) \right] \right\} \end{aligned} \quad (27)$$

$$\begin{aligned} W' = \frac{\alpha - a^{2x-1}}{[\gamma + \beta - b^{1/x}]^x} \left[\ln \left(\frac{a^2}{\gamma + \beta b^{1/x}} \right) \right. \\ \left. + \left(\frac{\beta b^{1/x} \ln(b)}{x(\gamma + \beta b^{1/x})} \right) \right] \end{aligned} \quad (28)$$

Eq. (13) can be written in the following form:

$$\Sigma Y(x_i) W' = \Sigma V(0) W W' \quad (29)$$

$$\begin{aligned} \Sigma Y(x_i) W' - \Sigma V(0) W \frac{\alpha a^{2x-1}}{[\gamma + \beta b^{1/x}]^x} \ln \left(\frac{a^2}{\gamma + \beta b^{1/x}} \right) \\ = \frac{1}{x} \Sigma V(0) W \frac{\alpha a^{2x-1}}{[\gamma + \beta b^{1/x}]^x} \left(\frac{\beta b^{1/x} \ln(b)}{\gamma + \beta b^{1/x}} \right) \end{aligned} \quad (30)$$

$$x = \frac{\Sigma V(0) W^2 \left(\frac{\beta b^{1/x} \ln(b)}{\gamma + \beta b^{1/x}} \right)}{\Sigma Y(x_i) W' - \Sigma V(0) W^2 \ln \left(\frac{a^2}{\gamma + \beta b^{1/x}} \right)} \quad (31)$$

Replacing all symbols with their definitions in Eq. (22), we get Eq. (14).

References

Abdelrahman, E.M., El-Araby, T.M., 1996–1997. An iterative approach to depth determination from moving average residual self-potential anomalies. *JKAU: Earth Science* 9, 17–27.

Abdelrahman, E.M., Sharafeldin, M.S., 1997. A least-squares approach to depth determination from self-potential anomalies caused by horizontal cylinders and spheres. *Geophysics* 62, 44–48.

Abdelrahman, E.M., Ammar, A.A., Sharafeldin, S.M., Hassanein, H.I., 1997a. Shape and depth solutions from numerical horizontal self-potential gradients. *Journal of Applied Geophysics* 37, 31–43.

Abdelrahman, E.M., El-Araby, T.M., Ammar, A.A., Hassanein, H.I., 1997b. A least-squares approach to shape determination from residual self-potential anomalies. *Pure and Applied Geophysics* 150, 121–128.

Abdelrahman, E.M., Ammar, A.A., Hassanein, H.I., Hafez, M.A., 1998a. Derivative analysis of SP anomalies. *Geophysics* 63, 890–897.

Abdelrahman, E.M., Hassanein, A.Gh., Hafez, M.A., 1998b. Interpretation of self-potential anomalies over two-dimensional plates by gradient analysis. *Pure and Applied Geophysics* 152, 773–780.

Abdelrahman, E.M., El-Araby, T.M., El-Araby, H.M., Ammar, A.A., Hassanein, H.I., 1999. Shape and depth solutions from moving average residual self-potential anomalies. *Kuwait Journal of Science & Engineering* 26, 321–336.

Abdelrahman, E.M., El-Araby, H.M., Hassanein, A.G., Hafez, M.A., 2003. New methods for shape and depth determination from SP data. *Geophysics* 68, 1202–1210.

Anderson, L.A., 1984. Self-potential investigations in the Puhimau thermal area, Kilauea Volcano, Hawaii. 54th Annual Internat.

- Mtg., Soc. Expl. Geophys., Expanded Abstracts, Soc. Expl. Geophys., Tulsa, Session: EM.3.5.
- Atchuta Rao, D., Ram Babu, H.V., 1983. Quantitative interpretation of self potential anomalies due to two-dimensional sheet-like bodies. *Geophysics* 48, 1659–1664.
- Atchuta Rao, D., Ram Babu, H.V., Silvakumar Sinha, G.D.J., 1982. A fourier transform method for the interpretation of self-potential anomalies due to the two-dimensional inclined sheets of finite depth extent. *Pure and Applied Geophysics* 120, 365–374.
- Bhattacharya, B.B., Roy, N., 1981. A note on the use of a nomogram for self-potential anomalies. *Geophysical Prospecting* 29, 102–107.
- Corwin, R.F., 1984. The self-potential method and its engineering applications; an overview. 54th Annual Internat. Mtg., Soc. Expl. Geophys., Expanded Abstracts, Soc. Expl. Geophys. Tulsa, Session: SP.1.
- Corwin, R.F., Hoover, D.B., 1979. The self-potential method in geothermal exploration. *Geophysics* 44, 226–245.
- Demidovich, B.P., Maron, I.A., 1973. *Computational Mathematics*. Mir Publ, Moscow.
- DeWitte, L., 1948. A new method of interpretation of self-potential data. *Geophysics* 13, 600–608.
- Fitterman, D.V., Corwin, R.F., 1982. Inversion of self-potential data from the Cerro-Prieto geothermal field Mexico. *Geophysics* 47, 938–945.
- Furness, P., 1992. Modelling spontaneous mineralization potentials with a new integral equation. *Journal of Applied Geophysics* 29, 143–155.
- Guptasarma, D., 1983. Effect of surface polarization on resistivity modeling. *Geophysics* 48, 98–106.
- Markiewicz, R.D., Davenport, G.C., Randall, J.A., 1984. The use of self potential surveys in geotechnical investigations. 54th Annual Internat. Mtg., Soc. Expl. Geophys., Expanded Abstracts, Soc. Expl. Geophysics., Tulsa, Session: SP.6.
- Meiser, P., 1962. A method of quantitative interpretation of self-potential measurements. *Geophysical Prospecting* 10, 203–218.
- Paul, M.K., 1965. Direct interpretation of self-potential anomalies caused by inclined sheets of infinite horizontal extensions. *Geophysics* 30, 418–423.
- Paul, M.K., Datta, S., Banerjee, B., 1965. Interpretation of self-potential anomalies due to localized causative bodies. *Pure and Applied Geophysics* 61, 95–100.
- Roy, S.V.S., Mohan, N.L., 1984. Spectral interpretation of self potential anomalies of some simple geometric bodies. *PAGEOPH* 78, 66–77.
- Satyanarayana Murty, B.V., Haricharen, P., 1985. Nomogram for the complete interpretation of spontaneous potential profiles over sheet-like and cylindrical two-dimensional sources. *Geophysics* 50, 1127–1135.
- Schiavone, D., Quarto, R., 1992. Cavities detection using the self-potential method. 54th Mtg., Eur. Assoc. Soc. Expl. Geophys., Abstracts. Eur. Assoc. Expl. Geophys., pp. 362–363.
- Shi, W., Morgan, F.D., 1996. Non-uniqueness in self-potential inversion. 66th Ann. Internat. Mtg., Soc. Expl. Geophys., Extended Abstracts, pp. 950–953.
- Stanley, J.M., 1977. Simplified magnetic interpretation of geologic contact and thin dike. *Geophysics* 42, 1236–1240.
- Yüngül, S., 1950. Interpretation of spontaneous polarization anomalies caused by spheroidal ore bodies. *Geophysics* 15, 237–246.